Received: 29 November 2021 | Revised: 4 February 2022 | Accepted: 20 February 2022

IET Generation, Transmission & Distribution

DOI: 10.1049/gtd2.12444

The Institution of Engineering and Technology WILEY

ORIGINAL RESEARCH PAPER

Damping torque coefficient analysis of PMSG-based WT with VSG control considering wind turbine dynamics

Tong Qu[1] | **Yujun Li**[1] | **Xiaotian Yuan**[1,2] | **Zhengchun Du**[1]

[1]Shaanxi Key Laboratory of Smart Grid, School of Electrical Engineering, Xi'an Jiaotong University, Xi'an, China

[2]School of Electrical and Electronic Engineering, Nanyang Technological University, Singapore, Singapore

Correspondence
Yujun Li and Zhengchun Du, Shaanxi Key Laboratory of Smart Grid, School of Electrical Engineering, Xi'an Jiaotong University, Xi'an 710049, China.
Email: yujunlizju@gmail.com; zcdu@xjtu.edu.cn

Funding information
National Natural Science Foundation of China-State Grid Corporation of China Joint Fund for Smart Grid, Grant/Award Number: U2066602; National Natural Science Foundation of China, Grant/Award Number: 51807150

Abstract

This paper expands the damping torque coefficient analysis (DTCA) for studying the small-signal stability of permanent magnet synchronous generator (PMSG)-based wind turbine (WT) under virtual synchronous generator (VSG) control with consideration of WT dynamics. Firstly, the typical VSG is implemented in the grid-side voltage source converter (GSVSC), which enables selfsynchronization without phase-locked loop (PLL). The maximum power point track (MPPT) algorithms are utilized to give the power reference for VSG. Then, the corresponding inertia and damping support can be provided by the kinetic energy of PMSG. Based on the established model, the DTCA is analytically conducted to not only reveal the key factors that influence the WT stability but also provide guidance for parameter tuning. As a result, it is important to find that the WT dynamics impair the damping and even lead to system instability. Moreover, the minimum value of VSG damping control parameter is analytically given to ensure the system stability under any load below the rated wind speed. Finally, the case studies considering one single PMSG connected to a large grid with and without inclusion of WT dynamics are performed and compared to demonstrate the accuracy of the proposed model and evaluate the applications of DTCA.

1 | INTRODUCTION

Wind energy has become the most promising renewable energy due to its abundant reserves, clean environmental protection and low cost. In recent years, the development and utilization of wind energy have become an important strategic choice for countries to achieve low carbon goals. Therefore, the wind energy conversion system (WECS) has received extensive attention in the research community [1, 2].

In the future, the effective inertia level and short-circuit ratio (SCR) of the power system will decrease significantly with the large-scale replacement of synchronous generators (SGs) and the rapid development of high proportion renewable energy integration [3]. For the traditional PLL-based grid-following control of variable speed wind turbines (VSWT), the maximum power point tracking (MPPT) strategy is utilized for efficiency reasons to ensure the wind energy harvest at medium or low wind speed [4]. However, the traditional MPPT-based active power control (APC) cannot provide inertia and damping support for the AC grid, which would further increase the frequency regulation burden of the low-inertia AC system. Moreover, the traditional PLL-based grid-following control may have difficulties in maintaining stable operation under weak AC system with low SCR. Plenty of works have reported the instability phenomenon [5–7] induced by the interactions between PLL and the weak grid.

1.1 | Related works

There are two basic control methods to improve the inertial response capability of grid-connected VSWT, namely, the virtual inertial (VI) control based on PLL and the virtual synchronous generator (VSG) control without PLL. For the VI control, an auxiliary controller with frequency feedback is introduced in the control loop [8, 9]. It uses DC link capacitor energy or WT rotor kinetic energy to realize virtual inertia and provide dynamic frequency support for the power grid. The VI control

based on optimized power point tracking (OPPT) [10] provides an improved power oscillation damping for the system which avoids the negative interaction between the inertial response and the MPPT control under conventional auxiliary differential control. Nevertheless, these controls are still implemented under the PLL-based vector control method and have the risk of system instability dominated by PLL.

To improve these, VSGs are proposed [11, 12] recently to promote frequency response characteristics of grid-connected VSWT and solve the instability in weak grid caused by PLL.

According to control objectives, VSGs can be classified as VdcQ-type VSGs and PQ-type VSGs [13]. VdcQ-type VSGs are realized by the equivalence between the electrical model of the DC-link capacitance in back-to-back converters and the mechanical model of the shaft in SGs [14, 15]. However, limited by the capacity of the DC capacitor in WECS, VdcQ-type VSGs may produce huge DC link voltage fluctuations under grid frequency disturbance.

PQ-type VSGs are realized by the APC [16]. The authors in [17–19] have developed some VSG models for grid-connected inverters, in which the grid synchronization function of VSG is mainly realized by simulating the second-order swing equation of SGs. This makes it possible for the distributed energy equipped with the above VSG to provide inertial frequency support for weak AC grid without PLL. In order to make VSWT have the grid-forming ability, several authors [20–24] explore the possibility of applying VSG controls in WECS, ref. [20] proposes a method that parallels the WT with an energy storage inverter that utilizes the VSG control. However, such a scheme requires additional energy storage devices, which increases the equipment cost of the wind farm. Ref. [21] studies the VSG control strategy in the load-shedding operation of the PMSG-based WT. The coordinated strategy of the overspeed control and the pitch angle control is proposed to provide the reserve capacity of the primary frequency regulation. However, the load-shedding operation reduces the power output from WTs and results in the waste of wind resources. The VSG schemes for PMSG-based WT under MPPT are reported in [22–24] to improve the inertia characteristics of WECS. Nevertheless, these studies have not considered the influence of WT dynamics and controls on the inertial response of WECS under load fluctuation. Wang et al. [25] develop the VSG scheme for DFIG-based WT to equip it with good stability and dynamic frequency support ability when connected to a low-SCR grid. They have discussed the impact of the captured wind energy's dynamics on the inertia characteristics and also point out that WT dynamics should be taken into account when analysing the inertial response of WECS. However, the impact of specific WT controls (e.g., the MPPT control and the pitch angle control) on the inertia and damping of VSG-equipped WTs was not analysed in depth. As found in this paper, the damping of PMSG-based WT is different from the original control parameters of VSG during system dynamic due to the coupling effect between the VSG control and WT's controls. Accordingly, the inertial response of WECS is different from that of SG. In some cases, poor damping will seriously threaten the stability of the WECS.

1.2 | Research gaps

From the above observations, it can be indicated that most VSG controls are designed and analysed without inclusion of WT dynamics. The coupling effect between the MPPT control and the active power control loop of VSG is not considered. There is little existing literature examining the roles of WT dynamics on the stability of VSG-embedded WTs from the perspective of DTCA, nor do they analytically provide a minimum value of VSG damping control parameter for ensuring the system stability.

1.3 | Main contribution

To bridge these gaps, the DTCA [26–28] is utilized to substantially evaluate the small-signal stability of PMSG-based WT under typical VSG control considering WT dynamics. The implementation of VSG control in PMSG-based WT is firstly discussed, where the MPPT algorithms provide power reference for VSG control, ensuring the grid-synchronization of WT without relying on PLL and enabling the damping and the inertial response of WT. Then, the DTCA is utilized to analytically examine the key factors, especially the WT dynamics, that may affect the small-signal stability of the system. Correspondingly, the synchronous torque and the damping torque of this system can explicitly evaluate the system stability with physical meanings. According to the analytical outputs of DTCA, it is very important to find that the WT dynamics may impair the system damping or even lead to instability issues. Moreover, the minimum value of VSG damping control parameter is further discussed with the purpose of making sure WT stability under any load at low or medium wind speeds, which can provide an important reference for the parameter tuning for VSG control in PMSG-based WT. Simulation results of one single PMSG connected to a large grid with and without consideration of WT dynamics are fully conducted and compared to verify the accuracy of the proposed analytical models and evaluate the influences of control and system parameters on the system stability.

2 | CLASSICAL VSG CONTROL FOR VSCS

Before discussing the impact of WT dynamics on the small-signal stability of grid-connected WT system with VSG control, the VSG realized in grid-connected VSC is introduced firstly. The dominated oscillation frequency and the damping ratio of grid-connected VSC system without considering the dynamics of the prime movers are derived in this section.

2.1 | Basic principle of VSG control

When only considering the inertia support and damping oscillation performance of grid-connected VSC system, according to the second-order swing equation of classical SG, the

relationship between the VSC voltage phase δ_c, the VSC voltage angular frequency ω_c, and the active power can be expressed as follows,

$$\frac{d\delta_c}{dt} = \omega_{base}(\omega_c - \omega_g)$$
$$2H_c\frac{d\omega_c}{dt} = P_c^{ref} - P_c - K_c(\omega_c - \omega_g) \quad (1)$$

where ω_{base} is the base frequency of the grid, which is 100π (rad/s), in addition, other variables are represented by the per-unit value unless otherwise specified; ω_g is the angular frequency of the grid, which is considered as 1.0 p.u. for the offset of the grid frequency usually doesn't exceed 1.6% during the stable-state operation; P_c^{ref} and P_c are the mechanical input power and the electrical output power of the VSG, respectively; H_c and K_c are the inertia time constant and the damping control parameter of the VSG, respectively. Write (1) in Laplace form, then the rotor angle position δ_c and the rotor speed ω_c of the VSG can be derived as follows,

$$\delta_c = \omega_{base}(\omega_c - \omega_g)/s \quad (2)$$

$$\omega_c = \omega_g - \frac{P_c - P_c^{ref}}{2H_c s + K_c} \quad (3)$$

The rotor angle position δ_c from (2) is the phase of modulation coefficient for pulse width modulation (PWM). The control in (3) enables the VSG to provide electro-mechanical oscillation damping for the grid via setting the damping control parameter K_c. It has the same function as the damping winding in SG but can be set artificially without limitations by the physical model. The above two equations together constitute the self-synchronization control loop of grid-connected VSC system without PLL.

The amplitude of the VSC voltage can be determined by the open-loop control as follows,

$$V_c^{ref} = V_{c(0)} \quad (4)$$

where V_c^{ref} and $V_{c(0)}$ are the reference value and the set value of the VSC voltage, respectively. In the scenario of the VSC connected to the weak grid, the AC voltage stability of grid-connected system is very important. Therefore, the VSC is required to have sufficient capacity and control speed to keep the AC voltage constant according to the reference value V_c^{ref} from (4). In order to simplify the small-signal model of grid-connected system, the dynamics of the VSC voltage amplitude controller are also ignored. Therefore the VSC voltage V_c is regarded as a constant value, that is, $V_c = V_{c(0)}$.

The VSG is realized in grid-connected VSC by (2)–(4). It has the same external characteristics as the classical second-order SG model.

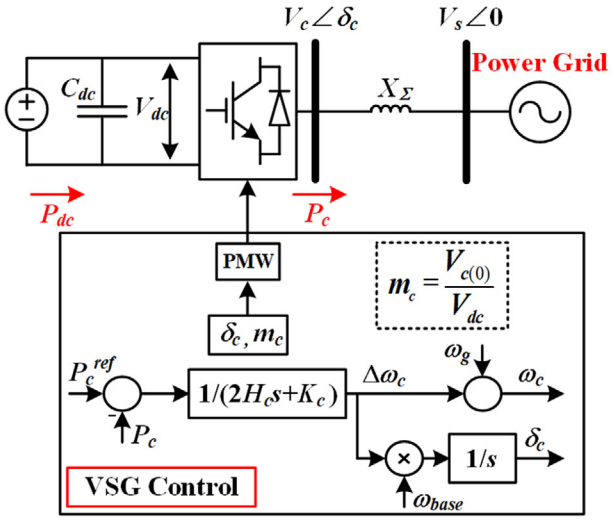

FIGURE 1 Grid-connected VSC system with VSG control

2.2 | Small-signal analysis of the VSG connected to a large power system

Figure 1 shows the simplest implementation of VSG control in grid-connected VSC. The AC side of VSC is connected to an infinite power system through the equivalent reactance X_Σ, which includes the VSC output reactance, the transformer reactance, the transmission line reactance and the grid equivalent reactance. The resistance between the infinite bus and VSC is not shown in Figure 1. $V_c\angle\delta_c$ and $V_s\angle 0$ represent the voltage vectors of VSC and the infinite bus, respectively. Therefore, the active power P_c exchanged in grid-connected VSC system without considering the loss can be expressed as,

$$P_c = \frac{V_c \cdot V_s}{X_\Sigma} \cdot \sin\delta_c \quad (5)$$

Write (1) and (5) into small-signal expression, leading to,

$$\frac{d\Delta\delta_c}{dt} = \omega_{base}\Delta\omega_c \quad (6)$$

$$\frac{d\Delta\omega_c}{dt} = \frac{1}{2H_c}\left(\Delta P_c^{ref} - \Delta P_c - K_c\Delta\omega_c\right) \quad (7)$$

$$\Delta P_c = \frac{V_{c(0)} \cdot V_s}{X_\Sigma} \cdot \cos\delta_{c(0)} \cdot \Delta\delta_c \quad (8)$$

where $\delta_{c(0)}$ is the steady-state value of the rotor angle position of the VSG, that is, the power angle of the grid-connected VSC system; Δ represents the small perturbation of state variables. If not considering the dynamics of the prime movers, the input power of the VSG in (7) is constant, that is, $\Delta P_c^{ref} = 0$. The system dynamic equation can be derived as follows,

$$2H_c\frac{d\Delta\omega_c}{dt} = -K_s\Delta\delta_c - K_c\Delta\omega_c \quad (9)$$

where K_s is a defined coefficient explained as (10). It represents the rate of the output power of the VSG to the rotor angle position of the VSG.

$$K_s = \frac{V_{c(0)} \cdot V_s}{X_\Sigma} \cdot \cos \delta_{c(0)} \tag{10}$$

Obviously, the synchronous torque and the damping torque of grid-connected VSC system are $K_s\Delta\delta_c$ and $K_c\Delta\omega_c$. Accordingly, K_s and K_c represent the synchronous power coefficient and the damping torque coefficient, respectively. Combine (6) and (9), the system dynamic equation of the grid-connected VSC system can be derived as follows,

$$2H_c\frac{d^2\Delta\delta_c}{dt^2} + K_c\frac{d\Delta\delta_c}{dt} + K_s\omega_{base}\Delta\delta_c = 0 \tag{11}$$

The dominated oscillation frequency and the damping ratio of the system can be described as follows,

$$f_d = \frac{\omega_d}{2\pi} = \frac{1}{2\pi} \cdot \sqrt{\frac{\omega_{base}K_s}{2H_c} - \left(\frac{K_c}{4H_c}\right)^2} \tag{12}$$

$$\zeta = \frac{K_c}{2\sqrt{2H_cK_s\omega_{base}}} \tag{13}$$

It should be noted from (12) and (13) that the dominated frequency and the damping ratio of the system is related to the control parameters of the VSG and the operating point of the grid-connected VSC system. More specifically, the larger the H_c, the slower the responding of the system to the disturbance and the worse the damping characteristics of the system. Moreover, ζ is in proportion to K_c. Just as the name of K_c, it represents the damping of the system to some extent.

Above analysis overlooks the impacts of the DC power source's dynamics on the damping of grid-connected VSC system. Actually, as for PMSG-based WT with VSG control, the rotor speed of WT changes in response to the disturbances of the grid frequency, which results in the change of P_c^{ref}. In the following section, the impacts of WT dynamics on the damping of grid-connected WT system are fully discussed.

3 | GRID-CONNECTED PMSG-BASED WT SYSTEM MODEL WITH VSG CONTROL UNDER MPPT

PMSG-based WTs consist of two full-rated backed-to-back converters which are connected through the DC-link capacitance. In the traditional PMSG-based WTs control, the WT provides the active power reference for the rotor side voltage source converter (RSVSC) by the MPPT control. Then, the active power from PMSG is modulated by the RSVSC. The GSVSC is used to maintain the DC-link voltage of the VSC. However, under such a control scheme, the PLL is required to track the phase angle information of the AC voltage at the point of common coupling (PCC). It may lead to system instability with improper PLL parameters when the GSVSC is connected to a high-impedance weak grid. To overcome the shortcomings induced by PLL, the GSVSC is controlled as a VSG, so that the inertial and frequency support can be exerted from PMSG-based WT during system disturbances.

In this section, the model of grid-connected WT system considering WT dynamics is constructed. The DTCA is utilized to analyze the impact of the additional torque introduced from WT dynamics on the inertia and the damping of grid-connected WT system.

3.1 | Basic operation principle of WTs with MPPT control

If the wind speed v_w is less than the rated wind speed v_{rated} of the WT, the mechanical power extracted by the WT can be described as follows with the actual value.

$$\begin{cases} P_W^M = \frac{\pi R^2\rho}{2} \cdot C_P(\lambda,\beta) \cdot {v_w}^3 \\ \lambda = \frac{\omega_r R}{v_w} \end{cases} \tag{14}$$

where P_W^M is the theoretical input wind power; ω_r is the rotor speed of WT; C_p is the wind energy utilization coefficient, which is relevant with the tip speed ratio, λ, and the pitch angle, β [degrees]; ρ and R are the air density and the blade radius of the WT, respectively. Accordingly, the optimal tip ratio can be indicated as follows at the certain wind speed v_w.

$$\begin{cases} \lambda_{opt} = \frac{\omega_{ropt}R}{v_w} \\ C_{P\max} = C_P(\lambda_{opt}, 0) \end{cases} \tag{15}$$

In such a condition, C_p gets its maximum. Combine (14) and (15), the maximum of theoretical input power expressed in the actual value can be derived as,

$$P_{w\max} = \frac{\pi R^2\rho}{2} \cdot C_{P\max} \cdot \frac{{\omega_{ropt}}^3 \cdot R^3}{{\lambda_{opt}}^3} = K \cdot {\omega_{ropt}}^3 \tag{16}$$

where

$$K = \frac{\pi R^5 \rho C_{P\max}}{2{\lambda_{opt}}^3} \tag{17}$$

As shown in Figure 2, The MPPT control of the WT only starts at medium or low wind speed. It regulates the rotor speed of WT at different wind speeds so that the wind power extracted by the WT can get its maximum.

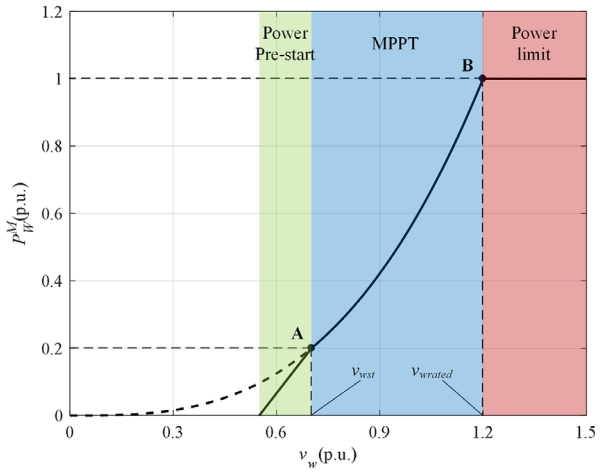

FIGURE 2 The relationship between wind speed and WT's mechanical input power

3.2 | Realization of VSG control in PMSG-based WTs

Different from the traditional control of PMSG-based WTs under MPPT, the active power reference from MPPT is provided to the GSVSC instead of the RSVSC, which means,

$$P_c^{ref} = P_{w\max} = k \cdot \omega_r{}^3 \tag{18}$$

where k is the normalization parameter. Specifically, to enable PMSG-based WTs to respond to the frequency disturbance of the system, the GSVSC controls the phase and magnitude of the VSG's AC voltage according to (2)–(4). And the RSVSC is utilized to maintain the DC-link voltage by the vector current (VC) control. The complete VSG control scheme for grid-connected PMSG-based WT is shown in Figure 3.

3.3 | System dynamic equations considering WT dynamics under MPPT

The WT dynamics without considering the rotor rotation damping can be expressed as follows, where ω_r is the rotor speed of WT; H_{WT} is the inertia time constant; $P_W{}^E$ is the output electrical power of PMSG.

$$2H_{WT} \cdot \omega_r \cdot \frac{d\omega_r}{dt} = P_W^M - P_W^E \tag{19}$$

To simplify the analysis, some assumptions about the model of grid-connected WT system are made as follows.

(i) Since the DC voltage control bandwidth is much smaller than the low-frequency oscillation frequency. For the time scale of the low-frequency oscillation mode, the DC voltage control of the RSVSC can be performed quickly. Therefore, the input power P_{dc1} of the DC-link capacitance is considered equal to the output power P_{dc2}.

(ii) Ignoring the losses from the resistance, the relationship of the power disturbance on each transmission line during system steady-state operation is as follows,

$$\Delta P_W^E = \Delta P_r = \Delta P_{dc1} = \Delta P_c \tag{20}$$

Combine (1) and (18), the output power of the VSG under MPPT can be written as follows,

$$P_c = k\omega_r^3 - 2H_c \cdot \frac{d\omega_c}{dt} - K_c \cdot (\omega_c - \omega_g) \tag{21}$$

Then, the following can be obtained by linearizing (19) and (21), respectively, with the help of (8), (10), and (20).

$$2H_{WT}\omega_{r(0)}\frac{d\Delta\omega_r}{dt} = -\Delta P_W^E + \Delta P_W^M = -K_s\Delta\delta_c + \Delta P_W^M \tag{22}$$

$$K_s\Delta\delta_c = 3k\omega_{r(0)}{}^2\Delta\omega_r - 2H_c\frac{d\omega_c}{dt} - K_c\Delta\omega_c \tag{23}$$

where $\omega_{r(0)}$ is the initial rotor speed of WT. Combine (6), (22), and (23), then write them in matrix form as follows,

$$\frac{d}{dt}\begin{bmatrix}\Delta\delta_c\\ \Delta\omega_c\\ \Delta\omega_r\end{bmatrix} = \begin{bmatrix}0 & \omega_{base} & 0\\ -\frac{K_s}{2H_c} & -\frac{K_c}{2H_c} & \frac{3k\omega_{r(0)}^2}{2H_c}\\ -\frac{K_s}{2H_{WT}\omega_{r(0)}} & 0 & 0\end{bmatrix}\cdot\begin{bmatrix}\Delta\delta_c\\ \Delta\omega_c\\ \Delta\omega_r\end{bmatrix} + \begin{bmatrix}0\\ 0\\ \frac{1}{2H_{WT}\omega_{r(0)}}\end{bmatrix}\cdot\Delta P_W^M \tag{24}$$

It is noted that when δ_c is shifted under a small disturbance of the system, ω_r will respond to this change immediately, which results in the input wind power P_W^M captured by the WT changing. However, the power offset ΔP_W^M around P_{wmax} is extremely small. Therefore, it is assumed that $\Delta P_W^M = 0$. Then, Write (24) into the Laplace form,

$$s \cdot \Delta\delta_c = \omega_{base} \cdot \Delta\omega_c \tag{25}$$

$$s \cdot \Delta\omega_c = -\frac{K_s}{2H_c} \cdot \Delta\delta_c - \frac{K_c}{2H_c} \cdot \Delta\omega_c + \frac{3k\omega_{r(0)}{}^2}{2H_c} \cdot \Delta\omega_r \tag{26}$$

$$s \cdot \Delta\omega_r = -\frac{K_s}{2H_{WT}\omega_{r(0)}} \cdot \Delta\delta_c \tag{27}$$

Combine (24)–(27), the system dynamic equation is derived as follows during system disturbances,

$$2H_c\frac{d\Delta\omega_c}{dt} = -K_s \cdot \Delta\delta_c - \left(K_c + \frac{3k\omega_{r(0)}}{2H_{WT}} \cdot \frac{K_s}{s^2} \cdot \omega_{base}\right) \cdot \Delta\omega_c \tag{28}$$

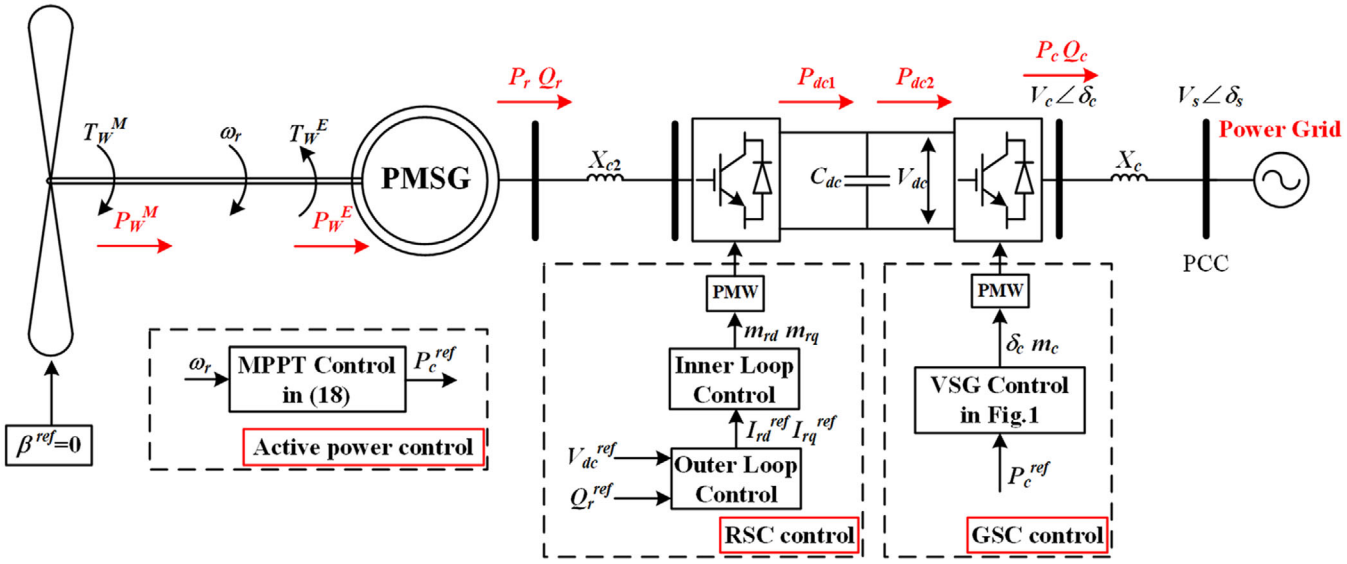

FIGURE 3 Control diagram of PMSG-based WT with VSG control

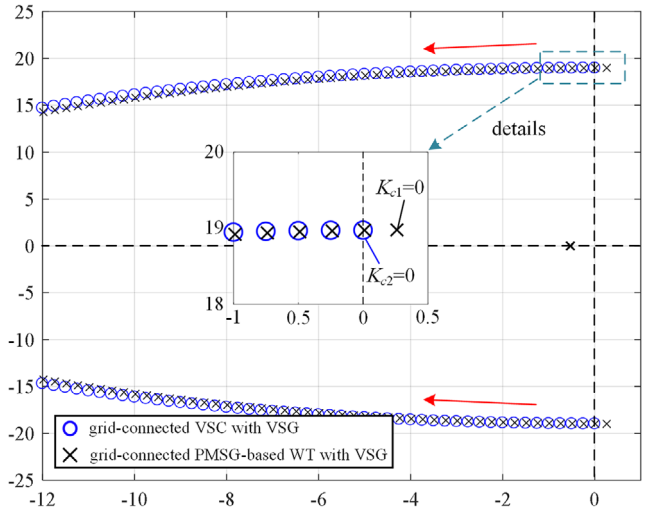

FIGURE 4 The Loci of systems' dominant eigenvalues as a function of K_c

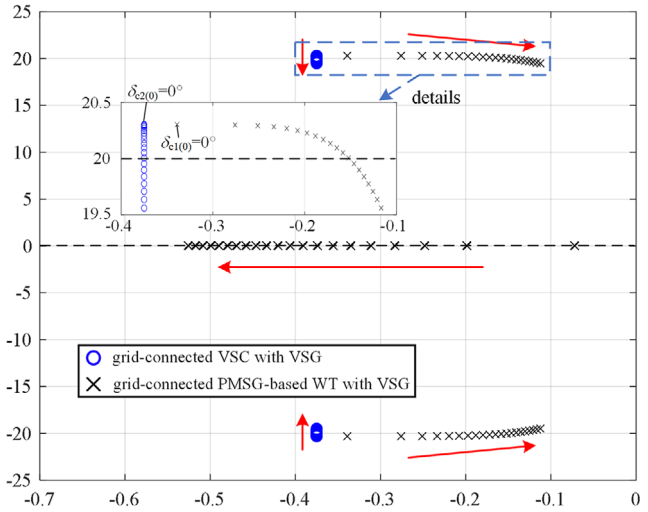

FIGURE 5 The Loci of systems' dominant eigenvalues as a function of $\delta_{c(0)}$

Compare (11) and (28), it is found that the term of the damping torque changes because of WT dynamics. Consider two grid-connected systems equipped with VSG. One of them is the PMSG-based WT system, the other is the grid-connected VSC system. They have the same external circuit topology with equal parameters. All the circuit and control parameters are listed in the Tables A1 and A2. It is easily found that the difference between the two systems is whether P_c^{ref} is constant during system oscillation. The root locus diagram of the two systems about K_c and $\delta_{c(0)}$ are shown in Figures 4 and 5, respectively. It can be found that with K_c or $\delta_{c(0)}$ varies in a wide range, the imaginary parts of two systems' dominant characteristic roots are almost equal, that is, the oscillation frequencies of two systems are similar. Therefore, the oscillation frequency of the PMSG-based WT system can be approximated as the dominant oscillation frequency f_d of the grid-connected VSC system in (12). Then, the system damping torque coefficient noted as K_c' can be derived as follows when $s = j\omega_d$.

$$K_c' = K_c - \frac{3k\omega_{r(0)}}{2H_{WT}} \cdot \frac{K_s}{\omega_d^2} \cdot \omega_{base} \tag{29}$$

Substitute the expression of the dominated oscillation frequency from (12) into (29), we have

$$K_c' = K_c - \frac{3k\omega_{r(0)}}{2H_{WT}} \cdot \frac{K_s}{\frac{\omega_{base}K_s}{2H_c} - \left(\frac{K_c}{4H_c}\right)^2} \cdot \omega_{base} \tag{30}$$

It is noted that $K_c' < K_c$, which means the WT dynamics deteriorates the system damping during system disturbances. K_c' is

not only related to the VSG damping control parameter K_c, but also determined by the initial rotor speed of WT, $\omega_{r(0)}$, and the inertia time constant H_c of the VSG.

3.4 | Impacts of reactive power droop control on stability

In the previous analysis, the VSC voltage is controlled as the constant V_c^{ref}. The inherent active power modulation characteristics of PQ-type VSGs force the rotor speed of WT to deviate from the MPPT state and the system damping torque is also weakened, which seriously threatens the dynamic stability of the system. In this section, to extend the existing VSG control, the reactive power droop control (RPDC) [29] as follows is applied in the GSVSC which emulates the excitation regulation of SGs.

$$m_c = k_Q(Q_c^{ref} - Q_c) \tag{31}$$

where Q_c^{ref} and $Q_{c(0)}$ are the reference and initial values of reactive power, respectively. k_Q is the droop factor of RPDC. According to the operation principle of VSC, the relationship between the VSC voltage and the DC voltage is expressed as,

$$V_c = m_c V_{dc} \tag{32}$$

As the system topology shown in Figure 3, the reactive power Q_c transported into the grid can be expressed as,

$$Q_c = \frac{V_c(V_c - V_s\cos\delta_c)}{X_\Sigma} \tag{33}$$

To further evaluate the impact of RPDC on the system inertial response, the following small-signal expression of (31)–(33) and (5) are derived, where K_{QV}, $K_{Q\delta}$ and K_{PV} are the corresponding coefficients depending on the initial operating conditions of the system.

$$\Delta m_c = -k_Q \Delta Q_c \tag{34}$$

$$\Delta V_c = \Delta m_c V_{dc(0)} \tag{35}$$

$$\begin{aligned}\Delta Q_c &= \frac{(2V_{c(0)} - V_s\cos\delta_{c(0)})\Delta V_c}{X_\Sigma} + \frac{V_{c(0)}V_s\sin\delta_{c(0)}\Delta\delta_c}{X_\Sigma} \\ &= K_{QV}\Delta V_c + K_{Q\delta}\Delta\delta_c\end{aligned} \tag{36}$$

$$\begin{aligned}\Delta P_c &= \frac{V_{c(0)}V_s\cos\delta_{c(0)}}{X_\Sigma}\Delta\delta_c + \frac{V_s\sin\delta_{c(0)}}{X_\Sigma}\Delta V_c \\ &= K_s\Delta\delta_c + K_{PV}\Delta V_c\end{aligned} \tag{37}$$

Combine (34)–(37), the relationship between ΔP_c and $\Delta\delta_c$ can be derived as follows,

$$\Delta P_c = \left(K_s - \frac{k_Q K_{Q\delta} V_{dc(0)}}{1 + k_Q K_{QV} V_{dc(0)}} K_{PV}\right)\Delta\delta_c \tag{38}$$

Compare (8) and (38), it is clear that the synchronous power coefficient of the grid-connected WT system decreases with the introduction of RPDC model. Nevertheless, the conditions $K_{QV} \gg K_{Q\delta}$ and $K_s \gg K_{PV}$ always exist in power systems, therefore, the synchronous power coefficient in (38) is very close to K_s. In summary, RPDC control has a weak influence on the inertial response of WECS and theoretically does not cause any deterioration of the system stability.

4 | ANALYSIS OF KEY FACTORS OF PMSG-BASED WT WITH VSG CONTROL ON SYSTEM STABILITY VIA DTCA

For further analysing the analytic relationship between K_c' and specific parameters in grid-connected system, the function of K_c' with the variables K_c and $\delta_{c(0)}$ are established in this section. Other parameters such as K_s and H_{WT} are generally considered to be unchanged once the selection of the transmission lines and generators are determined. In addition, The virtual inertia parameter, H_c, is easily constrained by the hardware and has significant impact on the system damping according to (13).

According to (1), (5), and (18), the relationship between the steady-state quantities is derived as follows,

$$P_{c(0)}^{ref} = k\omega_{r(0)}^3 = P_{c(0)} = a\cdot\sin\delta_{c(0)} \tag{39}$$

where the subscript (0) represents the variable is a steady-state value; The parameter a can be derived from (10) as follows,

$$a = \frac{K_s}{\cos\delta_{c(0)}} \tag{40}$$

Substitute (39) and (40) into (30), eliminate $\omega_{r(0)}$ and K_s, and record the damping torque coefficient K_c' as $f(K_c, \delta_{c(0)})$, which leads to,

$$f(K_c,\ \delta_{c(0)}) = K_c - m\cdot\frac{\cos\delta_{c(0)}\cdot(\sin\delta_{c(0)})^{(1/3)}}{\left(n\cdot\cos\delta_{c(0)} - K_c^2\right)} \tag{41}$$

where

$$\begin{cases} m = \dfrac{24k^{(2/3)}a^{(4/3)}H_c^2\cdot\omega_{base}}{H_{WT}} \\ n = 8H_c\omega_{base}\cdot a \end{cases} \tag{42}$$

The impact of K_c and $\delta_{c(0)}$ on the system damping torque coefficient is analysed as follows, respectively.

4.1 | Impact of the VSG control parameter K_c on K_c'

Taking the partial derivative of the function shown in (30) with respect to K_c, the sensitivity of the damping torque coefficient

to the parameter K_c can be expressed as,

$$\frac{\partial f}{\partial K_c} = 1 - m \cdot \frac{\cos \delta_{c(0)} \cdot (\sin \delta_{c(0)})^{(1/3)}}{\left(n \cdot \cos \delta_{c(0)} - K_c^2\right)^2} \cdot 2K_c \tag{43}$$

The result shows that the damping torque coefficient function in (43) decreases monotonically as K_c increases. Thus, there exists a maximum value of the system damping torque coefficient $K_{c\,\max}^{'} = f(K_{c\max}, \delta_{c(0)})$ when $\partial f/\partial K_{c\max} = 0$. But K_c is designed to be small due to energy consumption requirements which usually satisfies $K_c \ll K_{c\max}$. Therefore, the system damping torque coefficient is considered to increases with K_c.

If the parameter design of K_c is not reasonable, the system damping torque coefficient $K_c^{'}$ can get very small or even negative, which may cause grid-connected WT system instability. In order to guarantee the small-signal stability of the system, the damping torque coefficient function $f(K_c, \delta_{c(0)})$ must satisfy (44).

$$K_c - m \cdot \frac{\cos \delta_{c(0)} \cdot \left(\sin \delta_{c(0)}\right)^{(1/3)}}{\left(n \cdot \cos \delta_{c(0)} - K_c^2\right)} > 0 \tag{44}$$

where the typical value of $n{\cdot}\cos\delta_{c(0)}$ is usually much bigger than that of K_c^2. Thus, the minimum value of VSG damping control parameter can be derived by ignoring K_c^2 in (44),

$$K_{c\min} = \frac{m}{n} \cdot \left(\sin \delta_{c(0)}\right)^{(1/3)} = \frac{3H_c k^{\frac{2}{3}} \left(P_W^M\right)^{\frac{1}{3}}}{H_{WT}} \tag{45}$$

It can be seen from (45) that the minimum value of VSG damping control parameter $K_{c\min}$ to keep the critical stability of grid-connected PMSG-based WT system is affected by the system load. With the increase of the load, the $K_{c\min}$ increases and the steady-state stability margin decreases. When $P_W^M = 1.0$ p.u., the minimum value of VSG damping control parameter $K_{c\min s}$ can be derived as (46), where the system remains stable during any load if $K_c > K_{c\min s}$.

$$K_{c\min s} = K_{c\min}\big|_{P_M^W = 1} = \frac{3H_c k^{\frac{2}{3}}}{H_{WT}} \tag{46}$$

4.2 | Impact of the system power angle $\delta_{c(0)}$ on $K_c^{'}$

For ease of calculation, rewritten (41) as follows,

$$f\left(K_c,\ \delta_{c(0)}\right) = K_c - \frac{m/n \cdot \left(\sin \delta_{c(0)}\right)^{(1/3)} \left(n{\cdot}\cos \delta_{c(0)} - K_c^2\right)}{\left(n{\cdot}\cos \delta_{c(0)} - K_c^2\right)} - \frac{m/n \cdot K_c^2 \cdot \left(\sin \delta_{c(0)}\right)^{(1/3)}}{\left(n{\cdot}\cos \delta_{c(0)} - K_c^2\right)} \tag{47}$$

Taking the partial derivative of the function shown in (47) with respect to $\delta_{c(0)}$, the sensitivity of $f(K_c, \delta_{c(0)})$ to the system power angle $\delta_{c(0)}$ can be expressed as follows,

$$\frac{\partial f}{\partial \delta_{c(0)}} = -\frac{m}{3n} \cdot \left(\sin \delta_{c(0)}\right)^{(-2/3)} \cdot \cos \delta_{c(0)} \left(1 + \frac{K_c^2}{n{\cdot}\cos \delta_{c(0)} - K_c^2}\right) - \frac{m \cdot K_c^2 \cdot \left(\sin \delta_{c(0)}\right)^{(4/3)}}{\left(n{\cdot}\cos \delta_{c(0)} - K_c^2\right)^2} \tag{48}$$

If grid-connected system operates in the steady state, which means $0 < \delta_{c(0)} < 90°$, the function shown in (48) gets $\partial f/\partial \delta_{c(0)} < 0$. Therefore, $f(K_c, \delta_{c(0)})$ decreases monotonically with the increase of $\delta_{c(0)}$. when $\delta_{c(0)} = 0$, $K_c^{'}$ gets its maximum.

In summary, the PMSG-based WT at overload conditions provides less damping for grid-connected system. This is consistent with the analysis in the previous section that the overload condition deteriorates the damping of the system.

4.3 | Further discussion on the VSG control for PMSG-based WT

The main contribution of this paper is to examine the role of WT dynamics on the small-signal stability of the VSG-embedded wind energy integration system from the perspective of DTCA. Though it is found that the interaction between WT dynamic and VSG control may impair the system damping, the VSG control shows salient features for wind energy integration compared with traditional controls:

(i) A dedicated frequency measurement unit, that is, PLL is not required for VSG control, reducing the complexity of the overall control system. As a result, the negative damping induced by PLL is eliminated in weak grid, improving the stability of the parallel system.
(ii) The VSG-equipped WT achieves self-synchronization by emulating the rotor swing characteristics of SGs, equipping WT with grid-forming capability without PLL.
(iii) The auxiliary control functions, such as inertial response and damping controller can be embedded in the VSG control flexibly, enabling WT to give strong support for the weak AC system.
(iv) The VSG control has a wide range of applicability due to its general and simple control structure, which can be applied to any VSC-based generations and transmission lines, such as PMSG-based, DFIG-based WT and VSC-HVDC. It is relatively promising for future power system development under high percentage of renewable energy integration.

5 | SIMULATION STUDIES

To verify the phenomenon of the damping weakened by WT dynamics in grid-connected WT system with VSG control, the system where one single PMSG is connected to an infinite bus as shown in Figure 3 is established in MATLAB. All parameters of grid-connected PMSG-based WT system are listed in the Table A1.

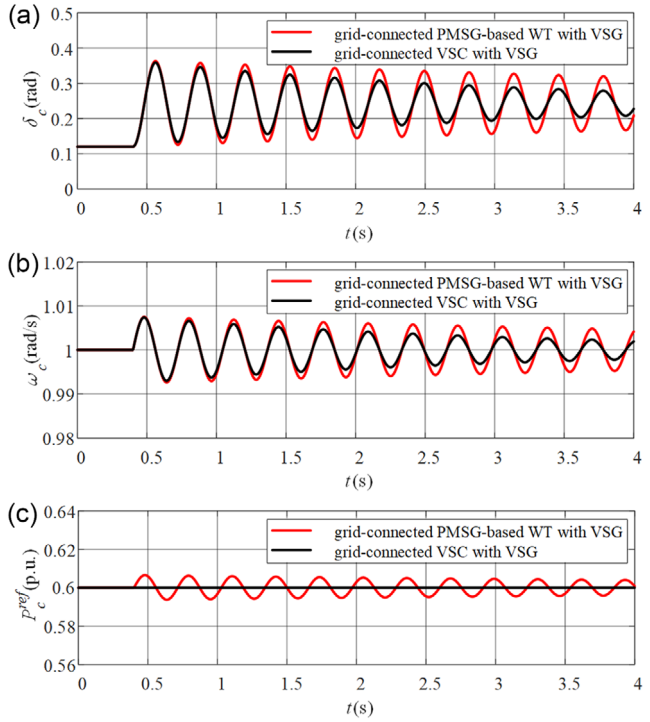

FIGURE 6 System dynamic response with sudden change of X_l from X_{l0} to X_{lf1} (a) the power angle of the system, (b) the frequency of the AC system, (c) the reference of the active power to the VSG

5.1 | Case 1: Impact of WT dynamics on the inertial response

As shown in Section 3, the PMSG consumes the rotor kinetic energy to provide damping for grid-connected system. However, different from the load-shedding operation of the WT where the active power reference P_c^{ref} provided to the VSG is constant, as for the MPPT control, P_c^{ref} is proportional to a cube of the rotor speed of WT. When the PMSG responds to the disturbance of the system, P_c^{ref} also changes, which will affect the grid-synchronization loop of the VSG and changes the inertial response process of the whole system. To illustrate such impact of WT dynamics on the inertial response of the system, Figure 6 compares the response of two systems with the VSG control to the sudden change in line parameters. One of the two systems is the grid-connected PMSG-based WT system under MPPT, the other is the grid-connected VSC system powered by a DC voltage source. As shown in the Table A2, the VSG control parameters of them are completely consistent. Specifically, the mechanical input power P_W^M of the PMSG in grid-connected WT system and the input power P_c^{ref} of the VSG powered by the DC voltage source are both 0.6 (p.u.). The other parameters are listed in the Table A1. When $t = 0.4$ s, the line reactance changes from X_{l0} to X_{lf1} to simulate single line disconnection. Figure 6a and b show the response of power angle and frequency of two grid-connected systems to the disturbance, respectively. It can be seen that the rate of change of frequency (ROCOF) $d\omega_c/dt$ of the first swing in the two systems are basically the same. However, compared with the grid-connected VSC system, the oscillation amplitude of the power angle and frequency of the grid-connected WT system is larger, and the time to return to the equilibrium point is also longer. Figure 6c shows the active power reference of two systems. Since the rotor speed of WT changes near the optimal operation point during the disturbance, according to (18), the active power reference P_c^{ref} output from MPPT changes, while the P_c^{ref} of the grid-connected VSC system remains unchanged. Therefore, the WT dynamics weakens the damping oscillations ability of the grid-connected WT system without affecting the inertia of the system. The simulation results also show that whether the system inertia is provided by the rotor kinetic energy of the PMSG or the DC voltage source, two VSGs with the same H_c show the same external characteristics to the AC system and provide equal inertia.

5.2 | Case 2: Impact of the control parameter K_c on the system damping

According to the analysis in Section 4, the damping of grid-connected PMSG-based WT system is determined by the VSG control parameter K_c and the system load level $\delta_{c(0)}$. In this section, the same disturbance as in Case 1 is considered. Other conditions remain unchanged except K_c. The impact of the variation of K_c on the damping of grid-connected system is investigated.

Figure 7 shows the root locus of the system about K_c. It can be seen that the system has three dominant characteristic roots. As K_c increases from 0, poles 2 and 3 shift to the left, which improves the stability and dynamic performance of the system. Pole 1 hardly moved so it has good damping. It is worth mentioning that the root locus curve in Figure 7 crosses the imaginary axis, which illustrates that the system becomes unstable when K_c is taken into a specific range. Therefore, as analysed in Section 4, there exists a minimum value of VSG damping control parameter $K_{c\min}$ to guarantee the small-signal stability of the system. The specific contents of this part will be discussed in Case 4.

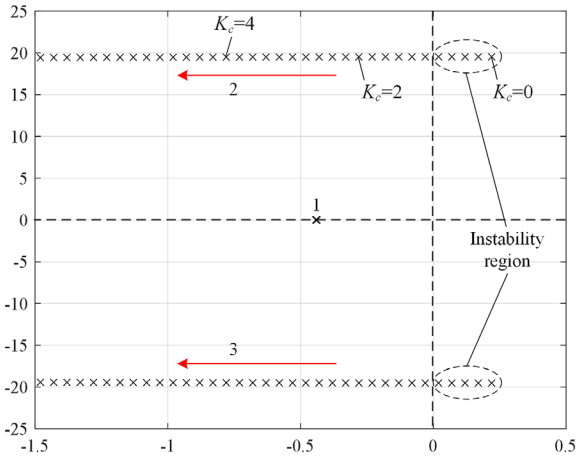

FIGURE 7 Loci of system dominant eigenvalues as a function of K_c

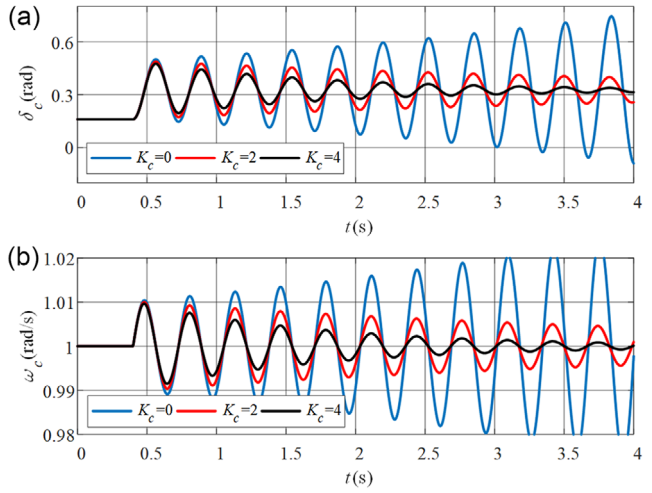

FIGURE 8 System dynamic response with sudden change of X_l from X_{l0} to X_{lf1} (a) the power angle of systems with different K_c, (b) the frequency of systems with different K_c

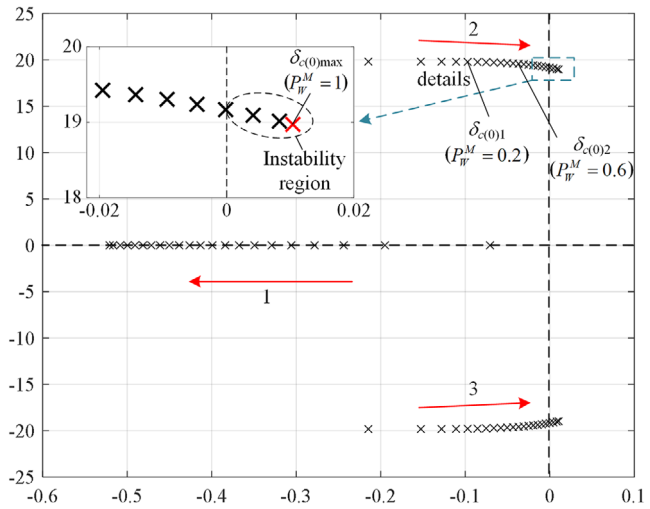

FIGURE 9 Loci of system dominant eigenvalues as a function of $\delta_{c(0)}$ (P_W^M)

Figure 8 shows the dynamic responses of the system when K_c is taken to 0, 2, and 4, respectively. It can be seen that with the increase of K_c, the grid-connected VSC system gradually changes from the small disturbance instability with $K_c = 0$ to stability with $K_c = 2$ and 4. Specifically, compared with the system with $K_c = 2$, the power angle and frequency of the system with $K_c = 4$ have smaller first swing amplitude and shorter steady-state recovery time, which illustrates that the grid-connected VSC system with large K_c has better damping and response performance.

5.3 | Case 3: Impact of the system power angle $\delta_{c(0)}$ on the system damping

In order to investigate the impact of the load level on the damping of grid-connected PMSG-based WT system, the same disturbance as in Case 1 is considered in this section, where $K_c = 1$, and other conditions remain unchanged except the mechanical input power P_W^M of the PMSG. As shown in Figure 2, the MPPT control only starts within the specific wind speed range ($v_{wst} < v_w < v_{wrated}$), which corresponds to $P_W^M \in [0.2, 1]$ p.u. According to (39), the $\delta_{c(0)}$ discussed here also has an corresponding operation interval. For ease of representation, the impact of $\delta_{c(0)}$ on system damping is indirectly investigated here by changing the P_W^M.

The root locus of the system about $\delta_{c(0)}$ (P_W^M) is shown in Figure 9, which indicates that there are three dominant characteristic roots in the system move with the change of P_W^M. As the P_W^M increases from 0.2 to 1 p.u., poles 2 and 3 shift to the right half plane and pole 1 shift to the left half plane. The overall system damping decreases by the influence of dominant complex roots 2 and 3 close to the virtual axis, so that the stability performance also becomes worse. When $P_W^M = 1$ p.u., the system loses its stability due to the root locus curve moving to the right half plane of the virtual axis.

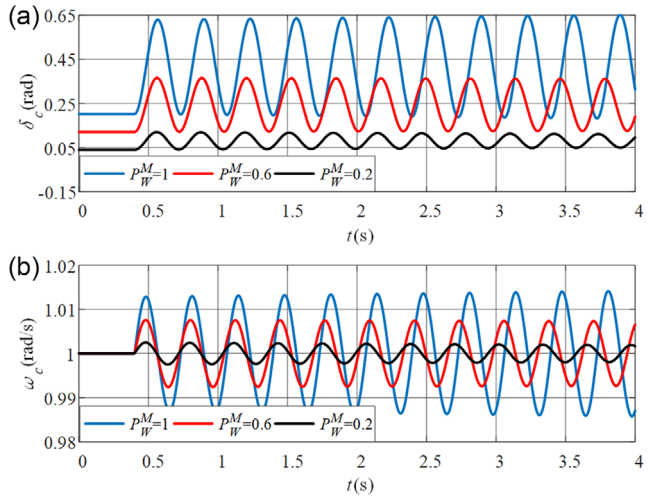

FIGURE 10 System dynamic response with sudden change of X_l from X_{l0} to X_{lf1} (a) the power angle of systems with different P_W^M, (b) the frequency of systems with different P_W^M

Figure 10 describes the disturbed dynamic response of the grid-connected WT system when P_W^M is 0.2, 0.6 and 1 p.u. respectively. It can be seen that the increasing amplitude oscillation occurs in the power angle and frequency of the system with P_W^M = 1.0 p.u., where the system loses its stability because of the insufficient system damping. In addition, compared with the system with P_W^M = 0.6 p.u., the power angle and frequency oscillation are suppressed faster in the system with P_W^M = 0.2 p.u., which indicates that the same VSG controller can provide relatively large damping when applied in grid-connected WT system under light load. Although two systems are stable during small disturbance, the system damping is still small, leading to a long time to recover to steady state. It can be seen that the dynamic performance of above three systems is not ideal when $K_c = 1$.

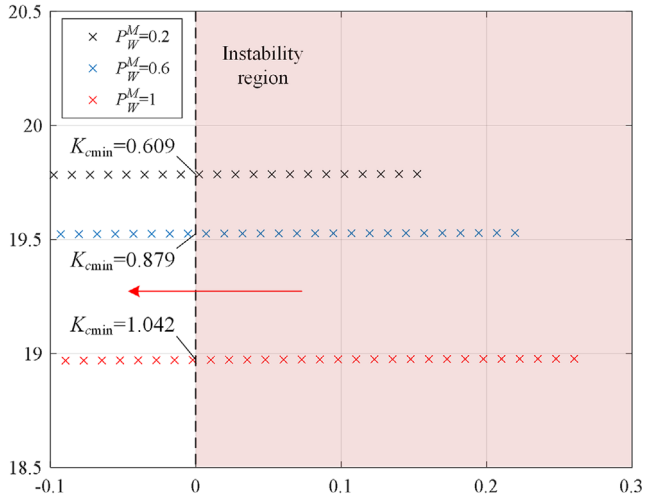

FIGURE 11 Loci of different load system dominant eigenvalues as a function of K_c

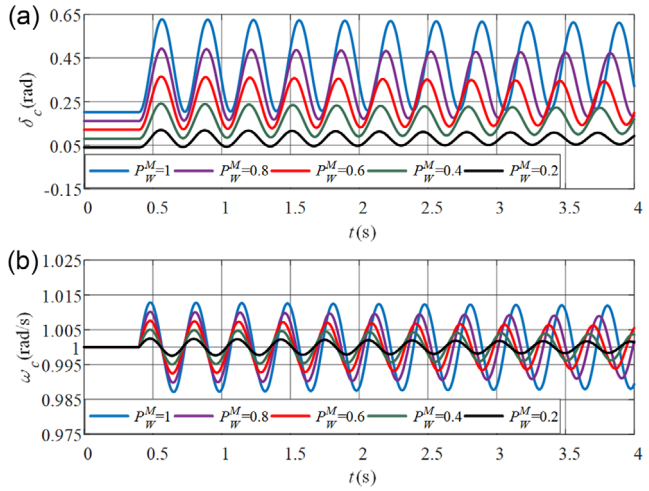

FIGURE 12 System dynamic response with sudden change of X_l from X_{l0} to X_{lf1} (a) the power angle of systems with different P_W^M, (b) the frequency of systems with different P_W^M

5.4 | Case 4: Impact of the power load on $K_{c\min}$

Figure 11 shows the root locus diagram of the grid-connected WT system about K_c at different load conditions. It can be seen that the minimum value of VSG damping control parameter $K_{c\min}$ increases with the increase of the system load, which means the stability margin of the system is decreasing.

Figure 12 describes the dynamic response of the system at different load conditions when the damping control parameter $K_c = 1.2$. According to (46), $K_{c\min s} = 1.042$, which means $K_c > K_{c\min s}$ are satisfied. It can be seen that the dynamic response of each grid-connected WT system shows the trend of oscillation attenuation and therefore the grid-connected WT system can keep its stability with $K_c = 1.2$.

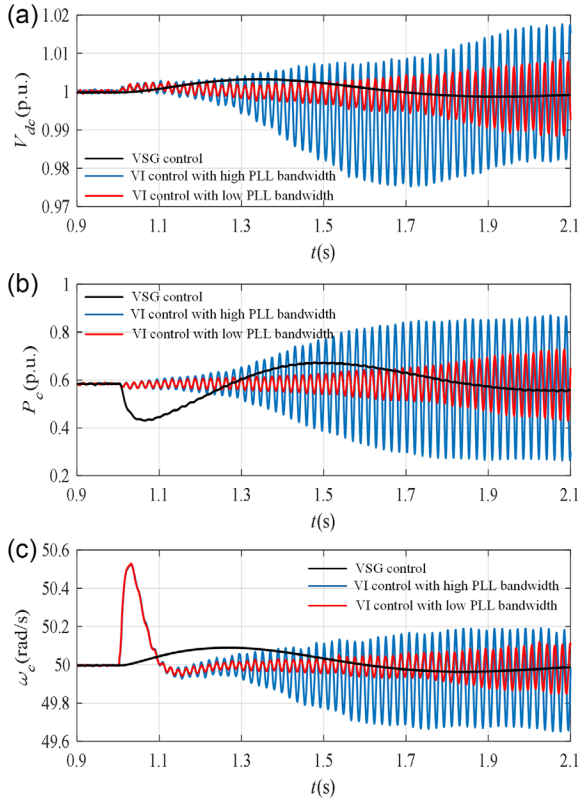

FIGURE 13 System dynamic response with sudden SCR decreased under different synchronization control (a) the DC capacitance voltage of WT, (b) the active power from WT, (c) the frequency of WT system

5.5 | Case 5: Comparison between the VSG control and the VI control

As illustrated before, there are two widely-used control methods for WECS, namely, the VI control and the VSG control. To perform the comparison simulation study, the typical and widely-utilized VI control based on PLL [9] for WECS is adopted in the comparative case study to show the priority of the VSG control.

Figure 13 shows the system dynamics of the WT integration system under system sudden short circuit ratio (SCR) decreased event, where the system SCR is changed from 5.0 to 1.2 (corresponding to the change in X_l from X_{l0} to X_{lf2}) at $t = 1.0$ s. Three different controls, that is, the VSG control, the VI control under high PLL bandwidth (25 Hz) and under low PLL bandwidth (16 Hz) are fully compared. To mitigate the impairment of WT dynamics on the system damping, the VSG damping control parameter is set as 8.

The AC grid becomes weaker as the SCR decreased. As clearly exhibited in Figure 13, when the system disturbance happens, the PLL dynamics bring negative damping to the overall WT integration system. Notably, the system under high PLL control bandwidth is more prone to be unstable compared with low PLL bandwidth, as observed in Figure 13. The DC-link voltage of WT cannot be well sustained during system dynamics due to the negative damping induced by PLL, as shown in Figure 13a. As a result, the output active power from GSVSC

and the grid frequency would exhibit unstable oscillations after system perturbations.

However, compared to the VI control, the VSG control shows better dynamic performance. As seen in Figure 13a, the DC-link voltage can be well maintained under VSG-based control. The system would experience a short period of oscillation until it recovers to a new steady-state equilibrium point, as shown in Figure 13b,c, whose dynamic responses are very similar to the typical SGs.

In summary, it can be concluded from the comparison case study that, the PLL-based VI control of WT integration system is only suitable for the strong AC grid (under high SCR), which may not operate well in weak AC system with low SCR and low inertial level. On the other hand, the VSG control with proper control parameters is relatively suitable for weak grid and exhibits robust characterises for effective wind energy integration, which is promising for the future power system with high proportion of renewable energy integration.

6 | CONCLUSION

In this paper, the small-signal stability of the PMSG-based WT with VSG control is examined via damping torque coefficient analysis considering WT dynamics. A simple and reliable VSG control for PMSG-based WTs is implemented, enabling the self-synchronization, inertial response and damping support of WT without PLL. Based on the established mathematical models of PMSG-based WT with VSG controls, the synchronous torque and the damping torque of grid-connected WT system are analytically derived at medium or low wind speed, which can not only explicitly reveal the key factors that may affect the system stability, but also offer guidance for parameter setting.

From the analytical outputs, it is very important to find that the WT dynamics would weaken the damping of the grid-connected WT system and might even result in system instability. Moreover, it is also concluded that the damping torque coefficient of the system is positively correlated with the damping control parameter K_c of the VSG in a large range and is negatively correlated with the system load level. Correspondingly, the minimum value of VSG damping control parameter for ensuring the stability of WT under any load level can be analytically obtained, which provides important guidance for the parameter setting of the VSG control in the PMSG-based WT.

The case studies of one PMSG-based WT under VSG controls with and without inclusion of WT dynamics are conducted and compared under different operating conditions, whose simulation results are consistent with the proposed analytical models.

ACKNOWLEDGEMENTS

This work was supported in part by the National Natural Science Foundation of China-State Grid Corporation of China Joint Fund for Smart Grid (No. U2066602), and in part by the National Natural Science Foundation (No. 51807150).

CONFLICT OF INTEREST

The authors do not have a conflict of interest.

DATA AVAILABILITY STATEMENT

The data that support the findings of this study are available from the corresponding author upon reasonable request.

REFERENCES

1. Aissou, R., Rekioua, T., Rekioua, D., Tounzi, A.: Robust nonlinear predictive control of permanent magnet synchronous generator turbine using dspace hardware. Int. J. Hydrogen Energy 41(45), 21047–21056 (2016)
2. Aissou, R., Rekioua, T., Rekioua, D., Tounzi, A.: Application of nonlinear predictive control for charging the battery using wind energy with permanent magnet synchronous generator. Int. J. Hydrogen Energy 41(45), 20964–20973 (2016)
3. Morren, J., Haan, S.W.H.D., Kling, W.L., Ferreira, J.A.: Wind turbines emulating inertia and supporting primary frequency control. IEEE Trans. Power Syst. 21(1), 433–434 (2006)
4. Amirnaser, Y., Reza, I.: Variable-speed wind-power system. Voltage-Sourced Converters in Power Systems: Modeling, Control, and Applications. IEEE, Piscataway, NJ (2010)
5. Hu, J., Huang, Y., Wang, D., Yuan, H., Yuan, X.: Modeling of grid-connected Dfig-based wind turbines for Dc-link voltage stability analysis. IEEE Trans. Sustainable Energy 6(4), 1325–1336 (2015)
6. Hu, J., Hu, Q., Wang, B., Tang, H., Chi, Y.: Small signal instability of Pll-synchronized type-4 wind turbines connected to high-impedance Ac grid during lvrt. IEEE Trans. Energy Convers. 31(4), 1676–1687 (2016)
7. Liu, J., Yao, W., Wen, J., Fang, J., Jiang, L., He, H., Cheng, S.: Impact of power grid strength and pll parameters on stability of grid-connected dfig wind farm. IEEE Trans. Sustainable Energy 11(1), 545–557 (2020)
8. Arani, M.F.M., El-Saadany, E.F.: Implementing virtual inertia in dfig-based wind power generation. IEEE Trans. Power Syst. 28(2), 1373–1384 (2013)
9. Li, Y., Xu, Z., Wong, K.P.: Advanced control strategies of pmsg-based wind turbines for system inertia support. IEEE Trans. Power Syst. 32(4), 3027–3037 (2017)
10. Wang, Y., Meng, J., Zhang, X., Xu, L.: Control of pmsg-based wind turbines for system inertial response and power oscillation damping. IEEE Trans. Sustainable Energy 6(2), 565–574 (2015)
11. Driesen, J. & Visscher, K.: Virtual synchronous generators. In: 2008 IEEE Power and Energy Society General Meeting - Conversion and Delivery of Electrical Energy in the 21st Century. Pittsburgh, PA (2008)
12. Visscher, K. & Haan, S. : Virtual synchronous machines (Vsg's) for frequency stabilisation in future grids with a significant share of decentralized generation. In: SmartGrids for Distribution, 2008. IET-CIRED. CIRED Seminar. Frankfurt (2008)
13. Huang, L., Xin, H., Zhen, W., Wu, K., Wang, H., Hu, J., Lu, C.: A virtual synchronous control for voltage source converters utilizing dynamics of dc-link capacitor to realize self-synchronization. IEEE J. Emerging Sel. Top. Power Electron. 5(4), 1565-1577 (2017)
14. He, J., Wu, K., Huang, L., Xin, H. & Wang, H. : A coordinated control scheme to realize frequency support of pmsg-based wind turbines in weak grids. In: 2018 IEEE Power & Energy Society General Meeting (PESGM). Denver, CO (2018)
15. Li, Y., Yuan, X., Li, J., Xiao, H., Du, Z.: Novel grid-forming control of permanent magnet synchronous generator-based wind turbine for integrating weak ac grid without sacrificing maximum power point tracking. IET Gener. Transm. Distrib. 15(10), 1613–1625 (2021)
16. Othman, M.H., Mokhlis, H., Mubin, M., Talpur, S., Ab Aziz, N.F., Dradi, M., Mohamad, H.: Progress in control and coordination of energy storage system-based vsg: A review. IET Renewable Power Gener. 14(2), 177–187 (2020)
17. Zhong, Q.-C., Nguyen, P.-L., Ma, S.: Self-synchronized synchronverters: Inverters without a dedicated synchronization unit. IEEE Trans. Power Electron. 29(2), 617–630 (2013)
18. D'Arco, S., Suul, J.A., Fosso, O.B.: A virtual synchronous machine implementation for distributed control of power transformers in smartgrids. Electr. Power Syst. Res. 122(6), 180–197 (2015)
19. Guan, M., Pan, W., Jing, Z., Hao, Q., Xiang, Z.: Synchronous generator emulation control strategy for voltage source converter (Vsc) stations. IEEE Trans. Power Syst. 30(6), 3093–3101 (2015)

20. Huang, S., Wang, T., Jin, M. & Ji, T. : Analysis of dynamic interaction in wind-storage virtual synchronous generator integrated system. In: 2021 4th International Conference on Energy, Electrical and Power Engineering (CEEPE). Chongqing, China (2021)
21. Bao, G., Li, Y., He, X. & Liu, F. : Virtual synchronization control strategy of direct drive permanent magnet wind turbine under load shedding operation mode*. In: 2019 IEEE International Conference on Robotics and Biomimetics (ROBIO). Dali, China (2019)
22. Ge, Y., Sun, Y., Liu, C., Yang, X., Sun, T.: Active support control strategy of permanent magnet synchronous wind turbine and its adaptability analysis under weak grid. In: *2019 22nd International Conference on Electrical Machines and Systems (ICEMS)*. Harbin, China (2019)
23. Mi, D., Wang, T., Gao, M., Wang, Z.: Small signal stability analysis of pmsg-vsg and optimal design for control parameters. In: *2020 IEEE Power & Energy Society General Meeting (PESGM)*. Denver, CO (2020)
24. Zhong, Q.-C., Ma, Z., Ming, W.-L., Konstantopoulos, G.C.: Grid-friendly wind power systems based on the synchronverter technology. Energy Convers. Manage. 89, 719–726 (2015)
25. Wang, S., Hu, J., Yuan, X., Sun, L.: On inertial dynamics of virtual-synchronous-controlled dfig-based wind turbines. IEEE Trans. Energy Convers. 30(4), 1691–1702 (2015)
26. Demello, F.P., Concordia, C.: Concepts of synchronous machine stability as affected by excitation control. IEEE Trans. Power Appar. Syst. PAS-88(4), 316–329 (1969)
27. Qu, Z., Peng, J.C.H., Yang, H., Srinivasan, D.: Modeling and analysis of inner controls effects on damping and synchronizing torque components in vsg-controlled converter. IEEE Trans. Energy Convers. 36(1), 488–499 (2021)
28. Du, W., Fu, Q., Wang, H.F.: Power system small-signal angular stability affected by virtual synchronous generators. IEEE Trans. Power Syst. 34(4), 3209–3219 (2019)
29. Xu, X., Liang, D., Wang, Z., Li, D., Zhang, A., Xing, H.: The effect of dfig on electromechanical oscillation with combined reactive power damping control and virtual inertial control. In: *2019 IEEE 8th International Conference on Advanced Power System Automation and Protection (APAP)*. Xi'an, China (2019)

How to cite this article: Qu, T., Li, Y., Yuan, X., Du, Z. Damping torque coefficient analysis of PMSG-based WT with VSG control considering wind turbine dynamics. IET Gener. Transm. Distrib. 1–13 (2022). https://doi.org/10.1049/gtd2.12444

APPENDICES

TABLE A1 Parameters of the grid-connected PMSG-based WT system

Symbol	Item	Value
ω_{base}	Base value of frequency	100π (rad/s)
V_{sbase}	Base value of ac line voltage	3 (kV)
S_{base}	Base value of power	10 (MVA)
V_s	Rated voltage of infinite as system	1 (p.u.)
$V_{c(0)}$	VSC's set voltage	1.05 (p.u.)
X_{l0}	Equivalent reactance of the grid-connected WT system	0.2 (p.u.)
X_{lf1}	Equivalent reactance of the grid-connected WT system after operations	0.4 (p.u.)
X_{lf2}	Equivalent reactance of the grid-connected WT system after operations	0.83 (p.u.)
H_{WT}	Inertia time constant of the WT's shafting	2(s)
k	MPPT control coefficient	0.5787

TABLE A2 Parameters of the VSG controller

Symbol	Item	Value
H_c	Inertia time constant of the VSG	1
K_c	Damping power parameter of the VSG	1.5